High-energy overtone spectroscopy of some deuterated methanes

J. W. Perry,[a] D. J. Moll,[b] A. Kuppermann, and A. H. Zewail[c]
Arthur Amos Noyes Laboratory of Chemical Physics[d] California Institute of Technology, Pasadena, California 91125

(Received 7 November 1983; accepted 15 October 1984)

High-energy overtone photoacoustic spectroscopy of gas phase CHD_3 ($\Delta v_{CH} = 5,6$, and 7), CH_2D_2, CH_3D, and CH_4 ($\Delta v_{CH} = 6$) is reported. The overtone and combination bands of CHD_3 display partially resolved rotational structure with laser limited linewidths (~ 0.5 cm^{-1}). A combination sum analysis is used to generate excited state rotational constants B'. We present an analysis of the Fermi resonances of CHD_3 which indicates strong interactions of the CH stretch with degenerate bending modes. The relative intensities of the Fermi interacting states are in agreement with those calculated from an analysis based on frequency shifts and a two or three level model. However, the rotational B' constants are not explained by such simple models indicating further interactions with states as yet unobserved. An upper limit of 10 cm^{-1} is estimated for the splitting of the $|6,0\rangle_{\pm}$ local mode states for CH_2D_2, giving support to a description based on the local mode picture. For CH_3D and CH_4 the spectra are apparently congested by overlapping overtone and combination bands and perhaps other mechanisms not identified in this work. Generally, our results emphasize the importance of the interactions of CH stretching with CH bending motions.

I. INTRODUCTION

The high-energy vibrational states of polyatomic molecules have attracted much interest in recent years. Much of this interest stems from the relevance of these states and their dynamics to selective laser-induced vibrational photochemistry. Other phenomena whose understanding will certainly benefit from studies of high-energy vibrational states include radiationless relaxation and multiphoton excitation and dissociation. In regards to selective laser-induced chemistry, the ability to localize a large fraction of the dissociation energy in specific modes or bonds for periods of time about equal to reaction or collision times is the main qualitative prerequisite for possible selectivity.

The local mode model[1] (and the local mode picture) has been used widely in the description of high-energy X–H (X = C, N, O) vibrational states.[2] Refinements of the theory which include the effects of coupling of the X–H stretches in two or more oscillator systems[3–6] have consistently shown that high-energy states are most easily described within the local mode picture. The reason for this situation is that for X–H bonds, the interbond coupling is less than the diagonal bond anharmonicity. The splitting of the symmetrized states has been shown to decrease with increasing v_{XH}, resulting in increased localization at higher energy. Also, the intensity of the lowest energy state in each v_{XH} manifold typically increases, relative to other states in the manifold, with increasing v_{XH}.

Recently, new information on the nature of high-energy CH-stretching overtones has been obtained.[7] The polarizations of the CH-stretch overtones of durene (1,2,4,5-tetramethylbenzene) crystals have been measured and analyzed. Using the molecular conformation of durene determined by x-ray diffraction methods, the calculated polarizations and the spectral assignments were compared for several models of the vibrational states. The results were found to be consistent with the local mode model for the durene CH-stretching overtones.

From the studies of the band shapes of overtone transitions, information on the relaxation of the high-energy states of large polyatomic molecules has been obtained. For aromatic CH-stretching overtones the bandwidths are typically ≥ 50 cm^{-1} for high v_{CH},[7–9] implying ultrafast population relaxation times of ≤ 0.1 ps, for molecules in the gas phase or low temperature solid. Perry and Zewail[7] have shown that for the methyl CH-stretching overtones ($\Delta v_{CH} = 5$) of durene, the bands become quite narrow, ~ 20 cm^{-1} at low temperature (~ 2 K). This suggests that the relaxation of methyl CH stretches is slower than for aromatic CH stretches (linewidth ~ 100 cm^{-1}) and the greater widths were rationalized in terms of a larger effective density of states for the aromatic CHs.

In this paper we present spectroscopic studies of the high-energy CH-stretching states of a family of relatively small molecules, some of the deuteromethanes: CHD_3, CH_2D_2, CH_3D, and CH_4. The relatively low density of states and large rotational B constants of these molecules suggest that it should be possible to observe fairly well resolved and isolated bands from which much information

[a] Current address: Molecular Spectroscopy Division, National Bureau of Standards, Gaithersburg, MD 20899.
[b] Current address: Dow Chemical Company, Midland, Michigan 48640.
[c] Camille and Henry Dreyfus Foundation Teacher–Scholar.
[d] Contribution No. 6935.

on (ro)vibrational coupling and, perhaps, excited state structure could be obtained. The series of deuteromethanes studied here also provides a situation where in going from one to four CH bonds in the molecules we may evaluate the relative importance of inter-CH bond stretch coupling and CH-stretch coupling to other modes of these prototypical saturated aliphatic molecules.

II. EXPERIMENTAL

The spectra presented in this paper were obtained using a pulsed laser photoacoustic spectrometer. A detailed description of this apparatus will be given elsewhere,[10] but some of its characteristics as well as the sample preparation and data handling are summarized below.

A. Sample preparation

The materials used in this study were: CHD_3 and CH_3D, Stohler Isotope Chemicals, 99% atom D; CH_2D_2, Merck Chemical, 99% atom D; CH_4, J. T. Baker, ultrapure. These materials were used without further purification. The photoacoustic cell was evacuated to 1×10^{-6} Torr for at least 12 h before filling. The photoacoustic spectra of CHD_3 in the region of the $v = 5$ and 6 stretch overtones were obtained using a pressure of 370 Torr, while the reduced transition intensity of the $v = 7$ spectrum required a higher sample pressure and 1385 Torr was used. The spectra did not change over a period of several days. They showed sharp rotational structure, which is absent at our resolution in the corresponding CH_4, CH_3D, and CH_2D_2 spectra. We conclude that this sharp structure cannot be attributed to isotopic impurities, small leaks, or outgassing of the photoacoustic cell. The $v = 6$ overtone spectra of CH_2D_2, CH_3D, and CH_4 were taken at sample pressures of 330, 370, and 300 Torr, respectively.

B. Laser system

The laser system consisted of a Molectron MY-34 pulsed Nd:YAG laser and a Molectron DL-18 dye laser. The second or third harmonics of the amplified Nd:YAG output were used to pump dye solutions of Exciton oxazine 725, rhodamine 640, or coumarin 540A in methanol or ethanol. The oxazine 725 oscillator output was amplified once by a transversely pumped dye amplifier. The rhodamine 640 oscillator output was amplified by a longitudinally pumped dye amplifier. The coumarin 540A oscillator output was amplified by two consecutive transversely pumped dye amplifiers.

Individual pulse energies were monitored by measuring the light reflected off two consecutive thin quartz flat beam splitters with a Laser Precision RKP-335 pyroelectric detector. Laser pulse energies varied as a function of wavelength within the range between 2 and 15 mJ/pulse. Dye laser FWHM pulse widths were reported by the manufacturer to be about 4×10^{-9} s. The pulse repetition rate was 10 Hz.

Absolute wavelength calibration was carried out using an iron–neon hollow cathode discharge lamp dispersed by a 0.5 m Ebert-type monochrometer. The absolute accuracy of the wavelengths reported in this paper is ±0.5 Å while the accuracy of the wavelength differences important for determining rotational constants is ±0.2 Å. The bandwidth of the laser was $\sim 0.5\ cm^{-1}$.

C. Photoacoustic cell

The photoacoustic cell used in this study was similar to that of West *et al.*[11] Its design reflected the important criteria that (1) the microphone detector was positioned as close as possible to the laser beam to maximize the amplitude of the outward moving cylindrical pressure wave, and (2) scattered light striking the walls of the cell near the microphone was minimized to reduce the background signal produce by local heating of the cell walls.

The cell was constructed using 3/8 in. brass Swagelok fittings. A Knowles Electronics BT1759 miniature electret microphone with built-in FET preamp was attached with epoxy resin to the side of a brass 3/8 in. Swagelok tee having an inner diameter of 9/32 in. such that it was about 6 mm from the cell axis. Carefully cleaned quartz windows were mounted 6 cm away from the microphone and aligned so that both windows were exactly perpendicular to the laser beam.

The photoacoustic signal from the miniature electret microphone following the laser excitation pulse has characteristics similar to those described by Chin *et al.*[12] An initial peak associated with the cylindrical pressure wave reached the microphone approximately 65 μs after the laser pulse, followed by a complicated sequence of additional pulses and ringing due to scattered light phenomenon. The delay between the laser pulse and the initial photoacoustic signal varies linearly with the distance of the microphone to the axis of the laser beam and is determined by the speed of sound in the gas. The spectrum is generated by monitoring the amplitude of the first peak as a function of laser wavelength. This amplitude is a linear function of the energy per laser pulse.

Due to the high intensity associated with pulsed laser beams care was taken to minimize nonlinear optical effects. The dye laser beam diameter was nominally 8 mm and an aperture allowed only the central 5 mm of the beam to enter the cell. With this configuration a linear dependence of the photoacoustic signal with pulse energy was observed. The linear dependence of signals on pulse energy and the absence of low lying electronic states appropriate for inducing resonance enhanced multiphoton electronic excitation or stimulated Raman processes in the systems studied permits us to conclude that nonlinear effects in the measured overtone spectra were unimportant. An additional confirmation of the conclusion is given by the similarity between our pulsed photoacoustic spectrum of CH_4 in the region near 619 nm and the long path absorption spectrum of Giver[13] and the cw photoacoustic spectrum of Stella *et al.*[14]

The effect of sample pressure on the photoacoustic spectra was also investigated; the only observed effect being an increase in photoacoustic signal with increasing pressure, without any change in the shape of these spectra.

Previous measurements of pressure broadening of CH_4 in the $2\nu_1$ band, the $3\nu_3$ band, and a line at 6190 Å all gave pressure broadening coefficients of approximately 0.087 cm^{-1}/atm.[15–17] If CHD_3 has similar pressure broadening coefficents the maximum expected pressure broadening in our experiments would be less than 0.2 cm^{-1}, well within the bandwidth of our laser.

D. Data handling

Electronic signals from the Knowles Electronics BT1759 electret microphone were limited to a frequency range of 300 to 10^4 Hz by an electronic filter and amplified by a factor of about 3×10^4. The peak of the first pressure wave was integrated by a differential gated integrator system with an integration window of 15 μs. Signals from the pyroelectric joulemeter were processed in a similar manner by a second integrator system.

A microcomputer system controlled the dye laser grating scan and digitized and stored the signals from both integrators every 0.1 Å. Each spectrum was scanned several times. The spectra were then laser-intensity-normalized and averaged. The CHD_3 $0 \rightarrow 5$, 6, and 7 CH-stretch experimental spectra of Figs. 1, 2, and 3, respectively, represent averages of 24, 36, and 120 laser shots for each 0.1 Å. Effective integration time constants and scan rates for the $0 \rightarrow 5$ and 6 spectra were adjusted so that the effective resolution was limited to ~0.5 cm^{-1} by

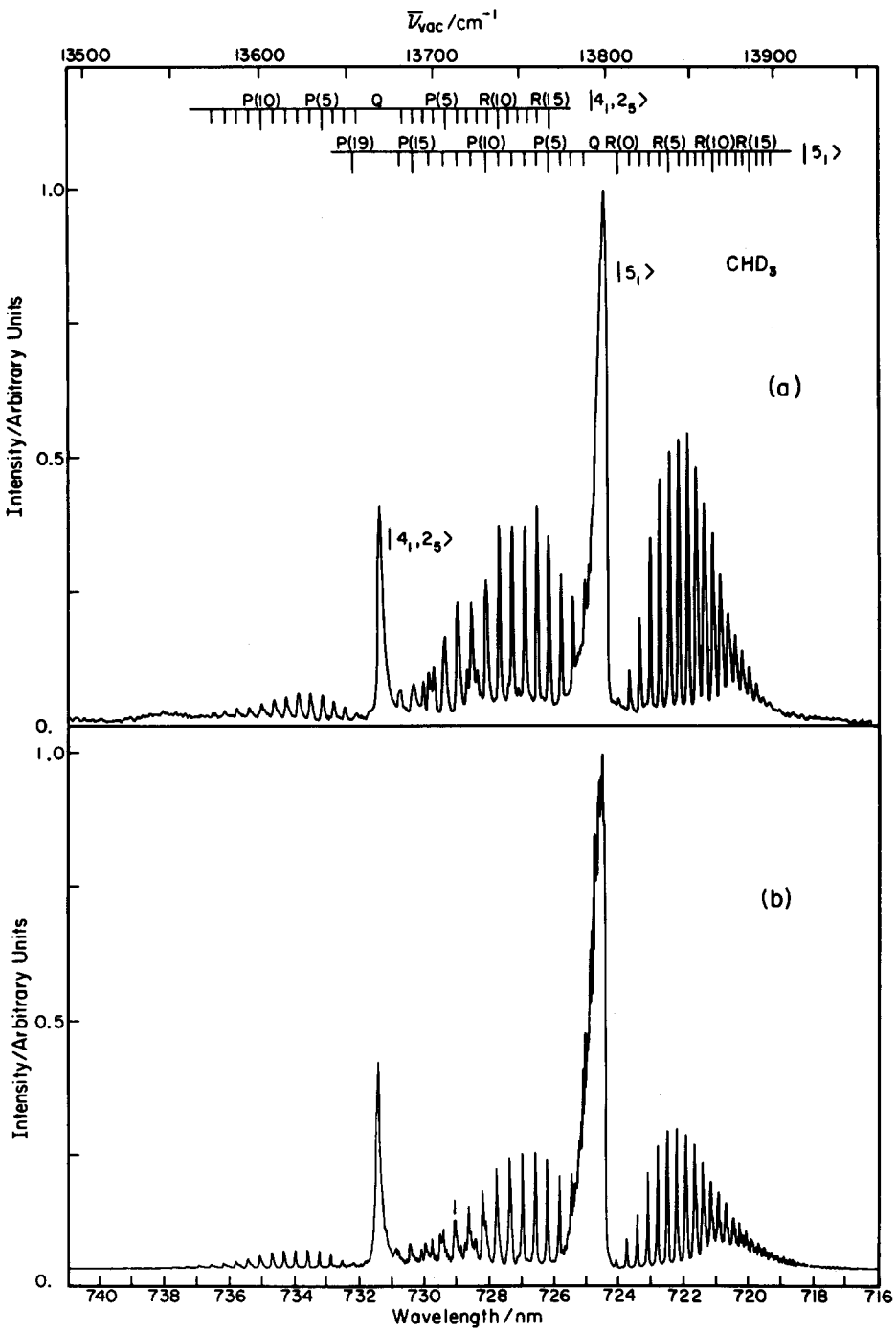

FIG. 1. Spectrum of CHD_3 in the region near the $\Delta v = 5$ CH-stretching overtone. (a) Pulsed laser photoacoustic spectrum of a 370 Torr sample at a temperature of ~25 °C; it is an average of two scans, each at 12 laser pulses for 0.01 nm wavelength interval. The signal intensities in this and all other experimental spectra presented in this paper were corrected for the variation of the incident laser light intensity with wavelength. (b) Theoretical fit to the experimental spectrum. The lower abscissa gives the air wavelength and the upper abscissa the vacuum wave number. The ordinates are in arbitrary units and have been normalized to unity at the top of the $|5_1\rangle$ Q branch. They represent signal intensity above the actual experimental base line without a background subtraction. The symbols $P(J)$, Q, and $R(J)$ correspond to rotational transition of $\Delta J = -1$, 0, and +1, respectively, where J is the rotational quantum number of the ground state. The symbols $|v_i, v_j\rangle$ represent the quantum numbers of the upper state.

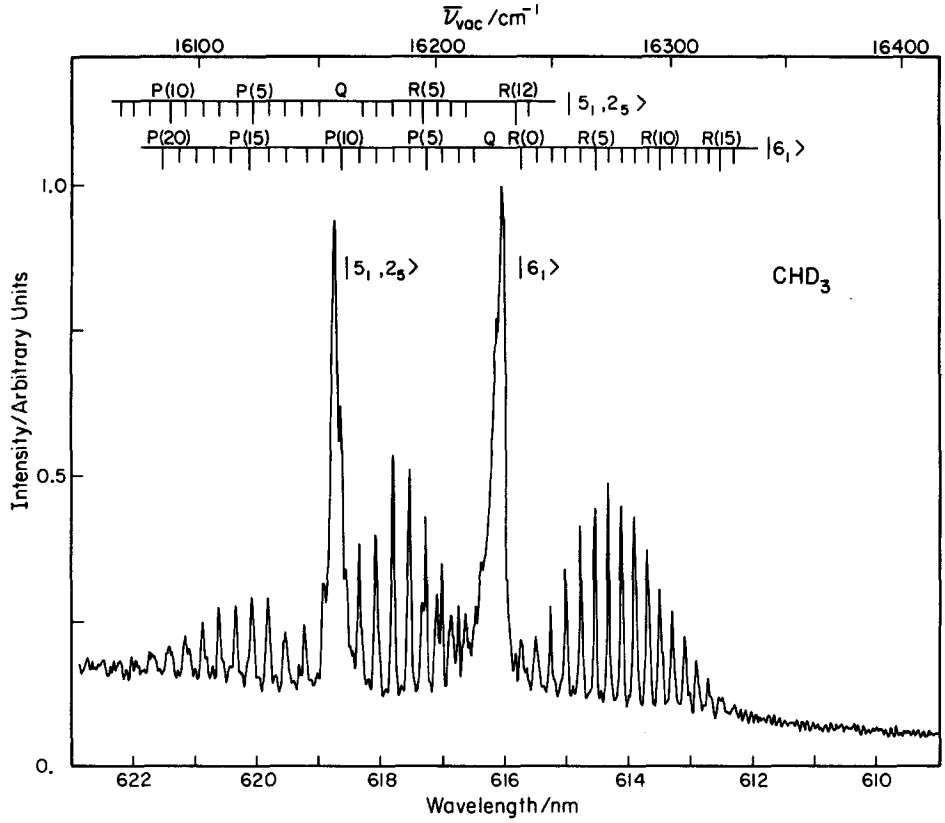

FIG. 2. Pulsed laser photoacoustic spectrum of CHD_3 in the region near the $\Delta v = 6$ CH-stretching overtone. The spectrum shown used a sample pressure of 370 Torr at ~25°C and is an average of three scans, each at 12 laser pulses per 0.01 nm wavelength interval. The lower abscissa gives the air wavelength, and the upper abscissa the vacuum wave number. The ordinate origin corresponds to approximately 90% of the observed signal at the right-hand side of the spectrum. This base line correction is due to the background signal from scattered light in the photoacoustic cell.

the laser bandwidth. The $0 \rightarrow 7$ transition was limited by the time constant used to ~0.7 cm^{-1}.

The CHD_3 photoacoustic spectra corresponding to the $v = 0 \rightarrow 6$ and 7 stretch overtones absorptions displayed large backgrounds which were approximately wavelength independent. We feel that the signal produced by light scattering inside the cell accounts for most of the constant background since the position of the axis of the photoacoustic cell with respect to the laser beam and the cleanliness of the quartz windows greatly affected the

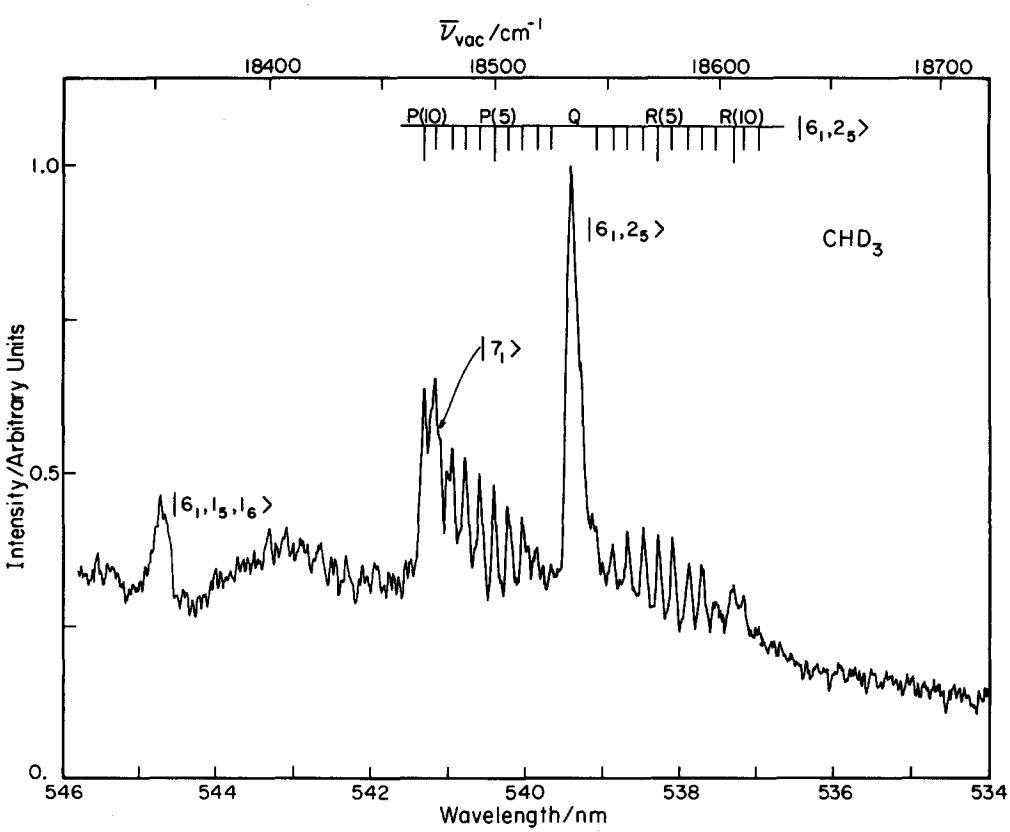

FIG. 3. Pulsed laser photoacoustic spectrum of CHD_3 in the region near the $\Delta v = 7$ CH-stretching overtone. The spectrum shown used a sample pressure of 1385 Torr at ~25°C and is an average of four scans, each at 30 laser pulses per 0.01 nm wavelength interval. The abscissae and the corrections for background and normalization of the ordinate are as described in the caption of Fig. 2.

magnitude of the background. Due to the uncertainty in the relative contributions of scattered light signals vs a real background absorption we have chosen for purposes of presentation to subtract off 90% of the apparent background in the $v = 0 \rightarrow 6$ and 7 spectra of Figs. 2 and 3. The $v = 0 \rightarrow 5$ experimental spectrum of Fig. 1(a) was left unchanged.

E. Approximate absorption cross sections for CHD_3

Approximate absorption cross sections for the various assigned vibrational transitions of CHD_3 are listed in Table I. The values given correspond to the peak of the central Q branch. These cross sections were estimated by considering the absolute photoacoustic signals, laser energy/pulse, and sample pressures, after calibrating our spectrum of CH_4 with the CH_4 absolute absorption cross sections of Giver[13] obtained for the same transition by a long path absorption method. The same deactivation efficiencies were assumed in CH_4 and CHD_3 for the purpose of this estimation. The absolute photoacoustic signal exhibits a strong dependence on the positions of the cell with respect to the laser beam, increasing as the microphone moves closer to that beam. When light actually strikes the cell walls, a dramatic increase in signal occurs. For each spectrum measured, an attempt was made to maximize the true absorption signal and minimize the scattered light signal. The resulting absolute calibration is therefore only approximate. The relative intensities of different vibrational states and their implications are discussed later.

A search was also made for state $|8_1\rangle$ in the region 487.7 to 476.7 nm, but without success. Signal to noise considerations in that spectral region indicate that state $|8_1\rangle$ or any other nearby combination bands must be at least a factor of 20 less than transitions to the $|7_1\rangle$ or $|6_1, 2_5\rangle$ states.

III. RESULTS AND DISCUSSION

A. CHD_3

1. High-energy overtone spectra

We were motivated to study the overtone spectroscopy of the deuteromethane series in part, as an attempt to identify various vibrational interactions which are significant for relatively small molecules at high vibrational energy. This series of molecules was chosen for the features of small size, high symmetry, and no strong polarizations, and for the fact that information on the low-energy spectroscopy and force field exists. Table II summarizes some spectroscopic parameters for CHD_3 from earlier work.

We begin with a consideration of the high CH-stretching overtones of CHD_3. This molecule is taken as a model system for separating interactions in the high-energy overtone region. We will be able to examine CH-stretch-normal mode coupling in the absence of interactions between degenerate CH-stretching states.

The question of whether the CH-stretching overtones of CHD_3 are better described from a local or normal mode model is not addressed in this work.[27] It can be argued that the difference between the two models is not great for CHD_3. The question amounts to whether the CD-stretch displacements can be neglected in comparison to the CH stretch. Based on the relative number (3 : 1) and relative masses (2 : 1) of D to H, it can be shown that the relative amplitude (CD/CH) would be quite small for CHD_3 even in the normal mode states. For the purposes of this work no further consideration of this question is necessary. We now turn to the experimental results.

In Fig. 1(a), 2, and 3 the CHD_3 stretching overtone spectra, which have been normalized for the laser intensity, are presented. The spectra are typically averages of only 3 or 4 scans each, and the signal-to-noise ratios are ~100, 50, and 30 for the $\Delta v = 5$, 6, and 7 regions, respectively. The drop in S/N reflects somewhat the decrease in absorption strength (described earlier) with increasing CH-stretching quantum number. Note the partially resolved rotational structure (discussed later) which corresponds, primarily, to the P, Q, and R branches for each vibrational band. Note also the presence of two main rovibrational band systems in the $\Delta v_{CH} = 5$ and 6 regions and three bands in the $\Delta v_{CH} = 7$ region.

With the observation of several bands near the CH-stretching overtones, it is apparent that there is a mixing or Fermi-resonance phenomenon involved which is distributing oscillator strength into the nearby states from the "pure" CH-stretching overtone. For CHD_3 there can be only one pure CH-stretching state at a given quantum level. This state is the corresponding overtone of the well-known fundamental[23,28] at 2992 cm^{-1} which is of A_1 symmetry in the C_{3v} molecular point group. Thus, all overtones of this mode are of A_1 symmetry also. Since the potential energy coupling terms must be totally symmetric,[9(a),30] the states involved in the Fermi resonance must likewise be of A_1 symmetry. From the point of view of assignment the problem is reduced to finding proper symmetry combination states or overtones in near resonance with the pure CH-stretching overtone. It is reasonable to restrict the consideration to combination states which can be expected to couple with the overtone through low-order potential coupling terms.

We will denote the vibrational eigenstates of CHD_3

TABLE I. Estimated absorption cross sections for CHD_3.

Vibrational band[a]	Photon energy (cm^{-1})[b]	Absorption cross section (cm^2)
$\|5_1\rangle$	13 799	$(3 \pm 1) \times 10^{-24}$
$\|6_1\rangle$	16 228	$(3 \pm 1) \times 10^{-25}$
$\|7_1\rangle$	18 473	$(7 \pm 3) \times 10^{-27}$
$\|4_1, 2_5\rangle$	13 668	$(1 \pm 0.5) \times 10^{-24}$
$\|5_1, 2_5\rangle$	16 157	$(3 \pm 1) \times 10^{-25}$
$\|6_1, 2_5\rangle$	18 534	$(1 \pm 0.5) \times 10^{-26}$
$\|6_1, 1_5, 1_6\rangle$	18 353	$(3 \pm 1) \times 10^{-27}$

[a] The notation is discussed in the text, Sec. III A 1.
[b] The photon energy of the cross section measurement is expressed in vacuum wave numbers, and corresponds to the peak of the Q branch of the specified vibrational band.

TABLE II. CHD_3 spectroscopic parameters from previous studies.[a]

Ground state parameters	
Parameter	Value (cm^{-1})
B'' [b]	3.279 053(61)
C'' [c]	2.629 7(3)
D''_J [b]	$5.010(19) \times 10^{-5}$
D''_{JK} [b]	$-4.030(69) \times 10^{-5}$
D''_K [c]	$1.8(3) \times 10^{-5}$

Excited state parameters (cm^{-1})

State[d]	$\bar{\nu}$	$B'-B''$	$C'-C''$	$D'_J-D''_J$	$D'_{JK}-D''_{JK}$	$D'_K-D''_K$
$\|1_3\rangle$[c]	1002					
$\|1_6\rangle$[c]	1035					
$\|1_4, -1_6\rangle$[e]	1237					
$\|1_5\rangle$[f]	1292.4992(8)	$4.641(11) \times 10^{-3}$	$2.0628(12) \times 10^{-2}$	$-1.29(3) \times 10^{-6}$	$-2.52(8) \times 10^{-6}$	$3.50(6) \times 10^{-6}$
$\|2_3\rangle$[c]	1988.87(3)					
$\|1_2\rangle$[h]	2142.5776	$-1.7549(19) \times 10^{-2}$	$-2.22(3) \times 10^{-2}$	$9.03(43) \times 10^{-7}$	$7.576(54) \times 10^{-6}$	$-1.0045(64) \times 10^{-5}$
$\|1_4\rangle$[c]	2250.88(10)	$-0.059(5)$	$-0.023(5)$	$2.3(2) \times 10^{-5}$	$7.1(5) \times 10^{-5}$	$-11.0(3) \times 10^{-5}$
$\|1_5, 1_6\rangle$[e]	2332					
$\|2_5\rangle$ (A)[g]	2564.6	0.01				
$\|2_5\rangle$ (E)[g]	2592.64	0.007	0.0449	$-5.0(8) \times 10^{-5}$	-3×10^{-5}	
$\|1_1\rangle$[h]	2992.33	-0.0179				
$\|1_3, 2_6\rangle$[e]	3051					
$\|1_2, 1_6\rangle$[e]	3181					
$\|1_4, 1_6\rangle$[e]	3283					
$\|1_3, 1_5, 1_6\rangle$[e]	3315					
	3327					
$\|1_2, 1_5\rangle$[e]	3456					
$\|1_1, 1_2\rangle$[i]	5135.04 (or 5134.84)					
$\|2_1\rangle$[j]	5865.02	-0.0381	-0.0181			
$\|3_1\rangle$[k]	8623.31	-0.0499		-1×10^{-5}		
$\|4_1\rangle$[k]	11266.94	-0.0641	-0.0350	6×10^{-6}	5×10^{-6}	

[a] Numbers in parentheses are the estimated errors in the last digit of the parameter values. Some correspond to 95% confidence limits and others are standard deviations. Please see the references indicated for details.
[b] Reference 18.
[c] Reference 19.
[d] The notation is described in the text.
[e] Reference 20.
[f] Reference 21.
[g] Reference 22.
[h] Reference 23.
[i] Reference 24.
[j] Reference 25.
[k] Reference 26.

in an occupation number representation as $|v_1, v_2, v_3, v_4, v_5, v_6\rangle$ where the quantum numbers are indexed in accord with Ref. 31. The CH stretch is labeled v_1. Only excited modes will be indicated, for example, the vth quantum CH-stretch level will be shown as $|v_1\rangle$.

We expect to find the appropriate combination levels for coupling to $|v_1\rangle$ in states of the form $|v_1 - 1, v_i, v_j\rangle$ or $|v_1 - 1, v_i\rangle$ with v_i and v_j being relatively small integers. The mixing of these states with $|v_1\rangle$ would require coupling terms of order $1 + v_i + v_i$ or $1 + v_i$ such as $V_{ij}^{(1+v_i+v_j)} \sim q_1 q_i^{v_i} q_j^{v_j}$ or $V_{1i}^{(1+v_i)} \sim q_1 q_i^{v_i}$ where q is the displacement coordinate in the harmonic oscillator basis. The total energy in the non-CH-stretching modes of the combination band must make up approximately one quantum of CH-stretch energy at the given v_1 level. The expression for the energy of a system of oscillators which includes doubly degenerate modes is given by the equation[29(b)]

$$E = \sum_i \bar{\nu}_i(v_i + d_i/2) + \sum_{\substack{i,j \\ i \geq j}} x_{ij}(v_i + d_i/2) \times (v_j + d_j/2) + \sum_{\substack{i,j \\ i \geq j}} g_{ij} l_i l_j, \quad (1)$$

where $\bar{\nu}_i$ are harmonic frequencies, d_i are degeneracies, x_{ij} are anharmonic constants, and the g_{ij} are vibrational angular momentum constants. The transition energy of an arbitrary pure overtone can be written (ignoring l-type splitting) as

$$\Delta E_i = \left(\bar{\nu}_i + x_{ii} d_i + \frac{1}{2} \sum_{j \neq i} x_{ij} d_j\right) v_i + x_{ii} v_i^2. \quad (2)$$

For the CHD_3 CH stretch this can be rewritten as

$$\Delta E_1 = \bar{\nu}_{\text{eff}} v_1 + x_{11} v_1^2, \quad (3)$$

where $\bar{v}_{\text{eff}}$ is the effective frequency and x_{11} is the diagonal anharmonic constant. The energy mismatch, one CH quantum, to be made up by the non-CH-stretch modes in the combination level must be approximately $\bar{\nu}_{\text{eff}} + x_{11}(2v - 1)$.

In Table III we list energies for the $CHD_3 \nu_1$ overtones obtained from this and previous work along with the best-fit calculated values based on Eq. (3). To help arrive at the assignments we have used the Birge–Sponer plot (see Fig. 4) for the $CHD_3 \nu_1$ overtones. The plot shows clearly that the higher energy band in the $\Delta v_1 = 5$ region falls very close to the extrapolated position of the best

TABLE III. Observed and calculated energies for CHD_3CH-stretch overtones.

State	ΔE_{obs}[a]	ΔE_{calc}[a,b]	Dev.
$\|1_1\rangle$	2 992.24	2 990.34	1.9
$\|2_1\rangle$	5 865.02	5 864.90	0.12
$\|3_1\rangle$	8 623.31	8 623.08	−0.37
$\|4_1\rangle$	11 266.9	11 266.68	0.22
$\|5_1\rangle$	13 801.2[c]	13 793.90	7.3[d]
$\|6_1\rangle$	16 230.1[c]	16 205.34	24.8[d]
$\|7_1\rangle$	18 473.0[c]	18 501.00	−28.0[d]

[a] Units are in vacuum wave numbers.
[b] Calculated using the parameters of the least squares fit of Eq. (3) to the wave numbers of the lower overtones (v = 1–4):

$$\bar{\nu}_{eff} = 3048.2(2)\ cm^{-1},\ x_{11} = -57.9(1)\ cm^{-1}.$$

[c] Bands observed in this work.
[d] Fermi resonance shifts.

straight line fit to the lower harmonics. This is consistent with our expectation that, in a weak coupling scheme, the highest intensity band should be the pure overtone. Here, the first order energies are not close enough for the levels to mix strongly. We assign this band as the pure overtone $|5_1\rangle$. As for the other band, we have considered possible combination states and we find two A_1 states which are close to the required energy and couple to $|5_1\rangle$ through low-order terms. These states are $|4_1, 2_5\rangle$ and $|4_1, 1_5, 1_6\rangle$ at 13 831 and 13 594 cm^{-1}, respectively, in zero-order (including diagonal anharmonicity), as calculated by using values from Table II and Ref. 31. Modes ν_5 and ν_6 are both of e symmetry, however, the levels $|2_5\rangle$ and $|1_5, 1_6\rangle$ split into A_1 and E sublevels of which the A_1 level may, with or without combination with the A_1 CH-stretch overtones, interact with A_1 CH-stretching levels. The spectra show (see Fig. 1) that there is a third level at lower energy than the other levels involved in the Fermi resonance near $\Delta v_1 = 7$. We take the combination band near $\Delta v_1 = 5$ to be $|4_1, 2_5\rangle$ which is the higher energy of the two combination bands. Note that this assignment suggests a large negative first-order shift of the combination band energy from the zero-order position (discussed later).

For the $\Delta v_1 = 6$ overtone region, two facts guide us in the assignment. First, we note again that the higher energy band lies closer to the extrapolation of the best fit line of the Birge–Sponer plot. Second, the shading of the Q branches is different for the two bands; the higher energy band is shaded to lower energy in the $\Delta v_1 = 5$ and 6 regions. This is taken as evidence that the higher energy bands correlate with the pure CH stretch and the lower energy bands correlate with combination states. However, the mixing is stronger at $\Delta v_1 = 6$, so the assignments here indicate only the parentage of the band. The higher energy band is therefore of $|6_1\rangle$ origin and the lower energy band is of $|5_1, 2_5\rangle$ origin for the $\Delta v_1 = 6$ region.

In the $\Delta v_1 = 7$ region the situation is somewhat different. The band closest to the Birge–Sponer line is the center band. Also, the Q branch at higher energy is shaded to high energy, in analogy with the $|4_1, 2_5\rangle$ and $|5_1, 2_5\rangle$ bands. These observations suggest that the band at higher energy in this region is actually of $|6_1, 2_5\rangle$ origin. The center band would be of $|7_1\rangle$ origin and the lower energy band is probably of $|6_1, 1_5, 1_6\rangle$ origin. Interestingly, this assignment, if correct, suggests that the band with the highest peak intensity in the $\Delta v_{CH} = 7$ region is in fact a combination band with one less CH-stretch quantum excited than in the pure overtone from which, presumably, oscillator strength is borrowed. We will return to a consideration of this point later, in the section on the analysis of the Fermi resonance.

The tuning and "crossover" of levels occur because of the larger anharmonic shift experienced by the pure overtone due to the larger CH-stretch quantum number. As v_{CH} increases by one, the anharmonic shift of the pure overtone $|v_{CH}\rangle$ relative to a combination band of the form $|v_{CH} - 1, \{v_i\}\rangle$ increases by $2x_{CH}$ (for a fixed $\{v_i\}$). Therefore, for a situation where at low v_{CH} the combination band is at lower energy than the overtone, there may be a crossing at higher v_{CH} of the combination and overtone states. Of course, this analysis neglects the possible off-diagonal anharmonic coupling of the modes, an effect which may introduce positive or negative relative shifts of the levels. The tuning of the Fermi resonance between CH-stretching states and combinations involving CH-bending modes has been observed in the overtone spectroscopy of the halomethanes,[6,32] haloethanes,[33] and of some lower alkanes.[34] Before discussing the discrepancy

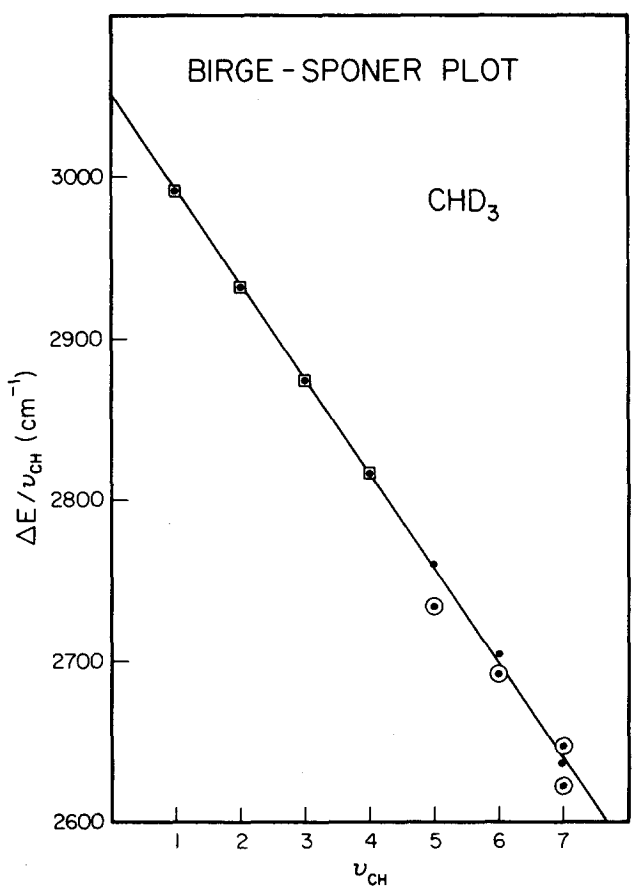

FIG. 4. Birge–Sponer plot ($\Delta E/v$ vs v) for CHD_3CH-stretching states. The symbols are defined as follows: ● our data, pure overtones; ⊡ previous data; ⊙ our data, combination bands.

between the zero-order and observed combination band positions we must consider the shifts due to the state mixing by Fermi resonance.

2. Analysis of the Fermi resonance

We now attempt an analysis of the Fermi resonance of the pure CH-stretching overtones with the CH-stretch–bend combination. The approximation of treating only the purely vibrational interaction between the levels is made; that is, we ignore Coriolis coupling to nearby E states. It is expected that the Fermi interaction of the totally symmetric overtone and combination states will dominate the relative intensities. We begin with the $\Delta v_1 = 5$ region.

Solution of the secular equation for the $|5_1\rangle$ and $|4_1, 2_5\rangle$ levels gives for the perturbed energies[29(a)]

$$E_\pm = \bar{E}_{12} \pm \tfrac{1}{2}(4W_{12}^2 + \delta^2)^{1/2}, \tag{4}$$

where the subscripts are defined as $1 \equiv |5_1\rangle$ and $2 \equiv |4_1, 2_5\rangle$, $\bar{E}_{12}$ is the average energy of the zero-order levels, W_{12} is the off-diagonal energy matrix element, and $\delta = (E_1^0 - E_2^0)$ is the difference in the zero-order energies. We measure spectroscopically the $E_\pm$ values and the intensities of the bands. The ratio of the intensities gives directly, in the case of two levels, the mixing coefficients for the interacting states. Unfortunately, the vibration-rotation bands that we have observed are overlapped, thus limiting the accuracy of the determined intensities. Another approach to determining the zero-order energies, interaction matrix elements, and mixing coefficients can be taken.

The zero-order pure overtone energies can be obtained from the extrapolation of the Birge–Sponer line. This is possible provided that terms in the potential energy of higher order than quartic do not have an appreciable contribution in the range of the extrapolation. Linear fits of the Birge–Sponer plots have been reported for many molecules[2] and up to very high vibrational quantum numbers ($\Delta v_{CH} = 9$).[8] We will therefore assume the extrapolation to be valid for CHD_3 at least up to $\Delta v_{CH} = 7$. From the difference in the observed energy of the pure overtone and the extrapolated value we obtained the Fermi resonance shift. Since the shifts due to the resonance interaction are of equal magnitude for the two-level problem, we can use the shift (7.3 cm^{-1}) of the observed $|5_1\rangle$ energy from the zero-order calculated energy to correct the observed $|4_1, 2_5\rangle$ energy. We are thereby able to obtain the zero-order energy for the combination band (see Table IV). The off-diagonal matrix element $|W_{12}|$, which can be obtained from Eq. (4), can now be calculated and is found to be 30 cm^{-1}.

The wave functions for the mixed states[35] are

$$\psi^+ = a|5_1\rangle + \sigma b|4_1, 2_5\rangle,$$
$$\psi^- = -\sigma b|5_1\rangle + a|4_1, 2_5\rangle, \tag{5}$$

where σ is the sign of W_{12} and $a^2 + b^2 = 1$. The expressions for the coefficients are

TABLE IV. Energies of CHD_3 $|v_1, 2_5\rangle$ CH-stretch–bend combinations.

State	ΔE_{obs}	ΔE_{corr}[a]	ΔE_{calc}[b]	$\Delta E^{(1)}_{obs}$[c]	$\Delta E^{(1)}_{calc}$
$\|4_1 2_5\rangle$	13 668	13 676	13 821	−156	−155
$\|5_1 2_5\rangle$	16 156	16 181	16 359	−177	−195
$\|6_1 2_5\rangle$	18 532	18 501[d]	18 770	−269	−234

[a] Fermi resonance corrected wave numbers.
[b] Calculated using the parameters given in footnote b of Table III and values in Table II.
[c] Value defined as $\Delta E_{corr} - \Delta E_{calc}$.
[d] Estimated from a numerical analysis of the three-level Fermi resonance analysis.

$$a = \left(\frac{\Gamma + \delta}{2\Gamma}\right)^{1/2},$$
$$b = \left(\frac{\Gamma - \delta}{2\Gamma}\right)^{1/2}, \tag{6}$$

where $\Gamma = (4W_{12}^2 + \delta^2)^{1/2}$. By using Eqs. (4) and (6) it can be shown that

$$b^2 = \left|\frac{E_1^0 - E_+}{E_+ - E_-}\right|. \tag{7}$$

The intensities of the transitions $|0\rangle \rightarrow \psi^+$ and $|0\rangle \rightarrow \psi^-$ are given by

$$I^+ \propto |\langle\psi^+|\mu_z|0\rangle|^2,$$
$$I^- \propto |\langle\psi^-|\mu_z|0\rangle|^2, \tag{8}$$

where μ_z is the component of the transition moment along the principal symmetry axis of the molecule. Expansion of the matrix elements gives

$$I^+ = a^2M_1^2 + b^2M_2^2 + 2\sigma abM_1M_2,$$
$$I^- = b^2M_1^2 + a^2M_2^2 - 2\sigma abM_1M_2, \tag{9}$$

where M_1 and M_2 are the zero-order transition matrix elements of the pure overtone $|5_1\rangle$, and the combination $|4_1, 2_5\rangle$, respectively. The transition moment operator is usually taken to be a single particle operator (sum of bond transition dipoles) which means that the combination band would have no zero-order intensity, i.e., M_2 would equal zero. If this is the case, then the ratio of the intensities is given by

$$I_{rel} = \frac{I_-}{I_+} = \frac{b^2}{a^2}. \tag{10}$$

Duncan et al.[35] have discussed some interesting effects which can occur if $M_2 \neq 0$. The interference term can lead to an asymmetry in the intensity borrowing such that $I^+ \neq I^-$ at the precise point of resonance. Since a and b are taken to be positive the sense of the asymmetry is determined by the sign of the interference term.

For now we take $M_2 = 0$. This allows us to use the simple expressions above for the mixing coefficients to calculate the relative intensities from the Fermi-resonance shift and the observed splitting of the bands. By using

Eq. (7) and the appropriate values from Tables III and IV one obtains $b^2 = 0.055$ and therefore $a^2 = 0.945$. The relative intensity was calculated, $I_{rel}^{calc} = 6 \pm 3\%$, and is somewhat lower than the observed value, $I_{rel}^{obs} = 18 \pm 8\%$, but agrees reasonably to the extent that the mixing is calculated to be fairly weak for this region. There are several factors which have been neglected and which may influence the calculated intensity, such as neglect of other levels which may be in weak resonance with the pure overtone, vibration-rotation interaction, or nonzero transition moment (M_2) of the combination band which could result, for example, from mixing with the $|4_1\rangle$ level or electrical anharmonicity.

Using the same method as above for the $\Delta v = 6$ region, we obtain $|W_{12}| = 35\ \mathrm{cm}^{-1}$, $a^2 = 0.66$, and $b^2 = 0.34$. The observed relative intensity is in good agreement with the calculated value, $I_{rel}^{obs} \approx 55 \pm 10\%$ and $I_{rel}^{calc} = 52 \pm 10\%$. Here the $|6_1\rangle - |5_1, 2_5\rangle$ mixing apparently dominates the relative intensity. Clearly there is strong mixing of the pure overtone and the combination band in this region. This leads, of course, to delocalization of the energy in the various modes involved (v_1 and v_5 in the present case).

In the $\Delta v_1 = 7$ region (Fig. 3) the Fermi resonance is more complicated due to the presence of at least one more sizable band than in the $\Delta v_1 = 5$ or 6 regions. The situation is complicated further due to severe overlapping of the band systems which results in a highly congested spectrum. It is not possible to estimate the relative band intensities with certainty without recourse to fitting the spectrum with a model. We will not pursue the analysis as such; rather, we wish to qualitatively explain the spectrum in terms of the assignment given above.

The standard treatment of the three-level resonance problem involves solution of a 3×3 secular determinant for the perturbed energies and for the mixed state wave functions. In the present case, implementation of this procedure is prevented due to a lack of knowledge of the various parameters.

We now define the abbreviations for zero-order states and interaction matrix elements in this region. The subscripts below will refer to zero-order states as follows: $1 \equiv |7_1\rangle$, $2 \equiv |6_1, 2_5\rangle$ and $3 \equiv |6_1, 1_5, 1_6\rangle$. For example, E_1^0 denotes the unperturbed energy of the $|7_1\rangle$ state and W_{13} is the interaction matrix element between $|7_1\rangle$ and $|6_1, 1_5, 1_6\rangle$. The only parameters which may be accurately calculated are E_1^0 and $|W_{12}|$. This leaves the problem undetermined since we have four unknowns E_2^0, E_3^0, W_{13}, and W_{23} and only three equations relating them. We resort to another level of approximation in order to explain the spectrum.

The assignment given earlier associates a combination band with the highest peak intensity feature (high-energy Q branch) in the $\Delta v = 7$ region. Although the relative integrated intensities may differ substantially from the relative Q branch peak heights we take them to be proportional for the sake of illustration. Thus, the observed relative intensities are approximately $0.15:0.35:0.50$ for $I_3:I_1:I_2$, respectively, where the subscripts refer to the perturbed levels of indicated parentage. One explanation for this intensity distribution would be as follows: the $|7_1\rangle$ and $|6_1, 2_5\rangle$ states are in very close resonance in zero-order and mix strongly given roughly equal intensities in the perturbed states. The $|6_1, 1_5, 1_6\rangle$ state, being closer to the $|7_1\rangle$ than the $|6_1, 2_5\rangle$ perturbed levels, now interacts with the perturbed overtone $|7_1\rangle$ and oscillator strength is distributed from the perturbed $|7_1\rangle$ level into $|6_1, 1_5, 1_6\rangle$, the mixing being less than the $|7_1\rangle - |6_1, 2_5\rangle$ mixing. This model explains qualitatively why the sum of the peak heights of $|7_1\rangle$ and $|6_1, 1_5, 1_6\rangle$ levels is about that of the $|6_1 2_5\rangle$ level. Even if there is a nonzero interaction between the $|6_1, 2_5\rangle$ and $|6_1, 1_5, 1_6\rangle$ levels, the conclusion of the above argument will hold qualitatively as long as

$$\left|\frac{W_{13}^2}{\Delta E_{13}^0}\right| \gg \left|\frac{W_{23}^2}{\Delta E_{23}^0}\right| . \tag{11}$$

One can now perform a simple numerical analysis of the three level resonance. First, the $|6_1, 1_5, 1_6\rangle$ level is ignored; we take $W_{13} = W_{23} = 0$, and the resulting 2×2 Fermi resonance is analyzed as before. We take the E_1^0 value to be that from the extrapolation of the Birge–Sponer plot. From this approximation we obtain $|W_{12}| \sim 30\ \mathrm{cm}^{-1}$. The combination state has crossed over to higher energy, in zero order, so now ψ^+ goes over into $|6_1, 2_5\rangle$ as $W_{12} \rightarrow 0$. We write the mixed state wave functions as

$$\psi^+ = a|6_1, 2_5\rangle + \sigma b|7_1\rangle,$$
$$\psi^- = -\sigma b|6_1, 2_5\rangle + a|7_1\rangle. \tag{12}$$

As before, we calculate the coefficients and get $a^2 = 0.53$ and $b^2 = 0.47$, indicating an almost equal mixture. If we allow for interaction with level 3, then assumptions about the values of the parameters are necessary to perform a numerical analysis. By a consideration of various approximations we find that $W_{13} \approx W_{12}$ if W_{23} is ignored. We also find that the amplitude of level 3 is smaller than the other bands and that the $|6_1, 1_5, 1_6\rangle - |7_1\rangle$ mixing is weaker than the $|6_1, 2_5\rangle - |7_1\rangle$ mixing. Further calculations, possibly involving exact diagonalization and least-squares fitting of the spectrum, are required to obtain more precise information.

The values of ΔE_{corr}, defined as ΔE_{obs} + FRS (Fermi resonance shift) for the $|v_1, 2_5\rangle$ state have been obtained and are given in Table IV. According to first-order perturbation theory, one expects for a combination band $|v_1, v_5\rangle$ a shift from the zero-order energy of the form

$$\Delta E_{15}^{(1)} = v_1 v_5 x_{15}, \tag{13}$$

where x_{15} is an off-diagonal anharmonic constant. In Table IV we list the observed shifts which were determined from the differences in the Fermi resonance corrected energy and the calculated energy. Using the shift of $|4_1 2_5\rangle$ to determine the constant x_{15} we obtain $-19.5 \pm 3\ \mathrm{cm}^{-1}$. This value is then scaled according to Eq. (13) for $|5_1, 2_5\rangle$ and $|6_1, 2_5\rangle$, and the results are listed in Table IV under $\Delta E_{calc}^{(1)}$. The errors are within $\sim$15% and we take this as reasonable, since the approach was the simplest

possible one. Note that the x_{15} value determined here is in good agreement with the anharmonic constant of Gray and Robiette: $x_{15} = -17.8$ cm^{-1}.[31] These authors have determined the anharmonic constants from a quadratic and cubic force field which was fit to relatively low-energy spectroscopic data.

3. Rotational analysis of partially resolved bands of CHD_3

CHD_3 is an oblate ($I_z > I_x = I_y$) symmetric top molecule belonging to the C_{3v} point group. Many of the degeneracies present in the CH_4 spherical top rotational spectrum are removed in CHD_3. In particular, parallel transitions between levels of A_1 symmetry in C_{3v} molecules are not influenced by first-order Coriolis effects, unlike perpendicular bands.[26]

Figures 1(a), 2, and 3 show pulsed photoacoustic spectra of CHD_3 in the region of the $v = 0 \rightarrow 5$, 6, and 7 overtones of the totally symmetric CH-stretching mode. Each spectrum displays two major vibrational bands, each containing a partially resolved P and R branch and a sharp central Q branch characteristic of a symmetric top parallel type transition.[29(c)] The overlap between the two bands becomes stronger for higher overtones, making the $v = 7$ spectrum congested enough that one Q branch is almost obscured by the other vibrational band's P

TABLE V. Observed wave numbers ($\bar{\nu}_{vac}$) for various CHD_3 bands.

State	J	$P(J)$ (cm^{-1})	$R(J)$ (cm^{-1})	State	J	$P(J)$ (cm^{-1})	$R(J)$ (cm^{-1})
$\|4_1 2_5\rangle$[a]	0	...	...		6	16 116.0	16 200.8
	1	13 661.8[b]	13 680.3		7	16 109.0	16 206.9
	2	13 665.5	13 687.6		8	16 102.2	16 212.9
	3	13 648.2	13 693.6		9	16 094.9	16 217.4
	4	13 641.9	13 699.7		10	16 088.2	...
	5	13 635.7	13 706.0		11	16 079.9[b]	...
	6	13 628.6	13 713.5[b]		12	16 072.7[b]	16 234.5[b]
	7	13 621.8[b]	13 719.1		13	16 067.8[b]	16 239.3[b]
	8	13 614.8	13 725.1				
	9	13 608.2	13 731.1	$\|6_1\rangle$[d]	0	...	16 236.6[b]
	10	13 601.0	13 737.3		1	...	16 243.0[b]
	11	13 593.8	13 742.9		2	16 216.3[b]	16 249.3
	12	13 587.0	13 748.7		3	16 209.8	16 255.4
	13	13 580.1	13 755.0		4	16 202.9	16 261.7
	14	13 573.3	13 759.5[b]		5	16 195.9	16 267.8
	15	...	13 766.6[b]		6	16 189.0	16 273.6
					7	16 182.0	16 279.2
$\|5_1\rangle$[a]	0	...	13 807.4[b]		8	16 174.9	16 284.8
	1	...	13 813.9		9	16 167.8	16 290.3
	2	13 787.6	13 819.9		10	16 160.0	16 295.4
	3	13 780.6	13 825.8		11	16 152.7	16 301.0
	4	13 773.6	13 831.7		12	16 145.1	16 306.3
	5	13 766.6	13 837.2		13	16 137.0	16 311.6
	6	13 759.5	13 842.9		14	16 129.5	16 316.7
	7	13 752.3	13 848.1		15	16 121.7	16 321.2
	8	13 744.8	13 853.2		16	16 113.9	16 327.8
	9	13 737.3	13 858.2		17	16 104.0	...
	10	13 729.8	13 863.0		18	16 099.4[b]	...
	11	13 721.5	13 867.8		19	16 092.1[b]	...
	12	13 713.5	13 872.5		20	16 084.6[b]	...
	13	13 705.3	13 876.5				
	14	13 696.7	13 881.0	$\|6_1 2_5\rangle$[e]	0	...	...
	15	13 688.1	13 885.0		1	18 524.9[b]	18 545.1
	16	13 679.4	13 889.2[b]		2	18 518.8	18 552.3
	17	...	13 892.8[b]		3	18 512.0	18 558.8
	18	...	13 896.5[b]		4	18 505.5	18 566.0
	19	13 651.4[b]	...		5	18 499.4	18 572.5
					6	18 492.9	18 579.1
$\|5_1 2_5\rangle$[c]	0	...	...		7	18 486.8	18 586.3[f]
	1	16 150.9[b]	16 169.4		8	18 481.0[b]	18 592.1[b]
	2	16 143.0	16 174.9[b]		9	18 473.5[f]	18 598.3[f]
	3	16 136.3[b]	16 182.0		10	18 468.7[f]	18 606.6[f]
	4	16 129.5	16 189.0		11	...	18 611.1[f]
	5	16 122.7	16 194.5		12	...	18 618.0[f]

[a] The reported values are accurate to ±0.6 cm^{-1}, and the differences are accurate to ±0.4 cm^{-1}.
[b] These points were not included in the combination sum analysis because of incomplete data or uncertainty in the position of the band.
[c] The reported values are accurate to ±0.8 cm^{-1}, and the differences are accurate to ±0.5 cm^{-1}.
[d] The reported values are accurate to ±0.08 cm^{-1}, and the differences are accurate to ±0.05 cm^{-1}.
[e] The reported values are accurate to ±1 cm^{-1}, and the differences are accurate to ±0.7 cm^{-1}.
[f] These points were not used in the combination sum analysis because they appeared to be strongly perturbed.

branch. A line listing of the various bands observed in this work is provided in Table V. We did not resolve the K-quantum number lines, but as discussed below the energies listed in Table V are approximately equal to the energy of the $K = 0$ line.

The rotational energy levels of an oblate symmetric top molecule in a specific vibrational level are given by

$$F(J, K) = BJ(J + 1) + (C - B)K^2 - D_J J^2(J + 1)^2 - D_{JK}(J + 1)K^2 - D_K K^4, \quad (14)$$

where B, C, D_J, D_{JK}, and D_K are the usual rotational constants.[29(d)] For a parallel band $\Delta K = 0$ and $\Delta J = 0$, ± 1 except that $\Delta J = 0$ is forbidden if $K = 0$.

A computer program utilizing Eq. (14) and the selection rules, appropriate Boltzmann factors, degeneracies, matrix elements, and spin statistics[29(e)] was written to generate symmetric top rotational spectra. The excellent signal-to-noise ratio in the spectrum of Fig. 1(a) suggested using a least-squares routine to adjust parameters in the spectral generation program to reproduce the experimentally observed spectrum. This was attempted using the CHD_3 ground state parameters of Jennings and Blass[18] and a FWHM linewidth of 0.5 cm^{-1}. Excited state parameters were adjusted from the $v = 4$ data of Bovey[26] until an approximate fit was observed. The least-squares routine was then allowed to make final adjustments on the excited state parameters.

Values for B' and ν_0 for the spectrum of Fig. 1(a) converged easily. These values along with constants generated by the combination sum approach described below are given in Table VI. The results of the two methods agree within the corresponding error limits. Other excited state parameters did not satisfactorily converge because experimental resolution prevented observation of individual K components, the presence of noise, and the possibility of excited state perturbations. Figure 1(b) shows a typical spectrum generated by the least squares routine corresponding to the region near the $|5_1\rangle$ and $|4_1, 2_5\rangle$ states of CHD_3. It should be noted that the ratios of the intensities of these two bands was one of the adjustable parameters in this fitting routine.

TABLE VI. CHD_3 spectroscopic constants from present study.[a]

Assignment[b]	$\bar{\nu}_0$ (cm^{-1})[c,d]	B' (cm^{-1})[e,d]
$\|4_1, 2_5\rangle$	13 668.1(1)	3.258(1)
	13 667.8(9)[f]	3.26(2)[f]
$\|5_1\rangle$	13 801.1(1)	3.2060(9)
	13 801.0(2)[f]	3.203(3)[f]
$\|5_1, 2_5\rangle$	16 156.4(2)	3.247(3)
$\|6_1\rangle$	16 230.07(9)	3.232(6)
$\|6_1, 1_5, 1_6\rangle$	18 353.0(5)[g]	...
$\|7_1\rangle$	18 473.0(5)[g]	...
$\|6_1, 2_5\rangle$	18 531.9(2)	3.301(7)

[a] Obtained by combination sum analysis unless otherwise stated. (See footnote f.)
[b] The notation is discussed in the text.
[c] Vibrational frequencies in vacuum wave numbers.
[d] Values in parenthesis are the uncertainties in the last digit, equal to 2 standard deviation units.
[e] B' is the rotational constant in vacuum wave numbers.
[f] Values obtained from least-squares fitting of the experimental spectrum.
[g] Insufficient structure was available for a rotational analysis to be performed. The value given corresponds to the position of the peak of the central Q branch.

Similar least-squares fits were attempted for the spectra in Figs. 2 and 3. The increased noise and large constant background (see Sec. II) limited the accuracy of these fits and a combination sum approach yielded more reliable results (see below). The synthesized spectra were used, however, to assign the individual J transitions in the congested regions of overlapping rotational features.

The resolution of the laser system (0.5 cm^{-1}) prevented the observation of single K components of specific J rotational transitions, although shading of individual J lines is observed at high values of J. Comparision of synthesized spectra at our experimental resolution with actual positions of the $K = 0$ lines indicated that the maximum of each J transition corresponds roughly to the position of the $K = 0$ transition.

Ground vibrational state rotational constants can be accurately determined even in the presence of excited state perturbations using the technique of ground state combination differences.[24] The combination difference $\Delta F''(J, K) = R(J - 1, K) - P(J + 1, K)$ involves transitions having the same upper state. Our photoacoustic spectra yield only approximate positions of the $K = 0$ lines and D''_J is much smaller than B''. Therefore, a plot of $[R(J - 1) - P(J + 1)]/(J + \frac{1}{2})$ vs $(J + \frac{1}{2})^2$ should yield a line with slope $8D''_J$ and intercept $4B''$. B'' was determined from spectra of the $|5_1\rangle$, $|6_1\rangle$, $|4_1, 2_5\rangle$, $|5_1, 2_5\rangle$, and $|6_1, 2_5\rangle$ states of CHD_3. The average value of B'' obtained in this way was 3.29 ± 0.03 cm^{-1}. The relatively large standard deviation is a result of the low resolution which prevents observation of individual K lines. Our value of B'' is consistent with the accurate value of 3.279 053 cm^{-1} of Jennings and Blass.[18]

The rotational constants of the upper vibrational state can be obtained by the combination sum $R(J - 1, K) + P(J, K)$.[26,29(f)] Figures 5–7 show plots of the combination sums $R(J - 1, 0) + P(J, 0)$ vs J^2 for the states $|5_1\rangle$, $|6_1\rangle$, $|4_1\rangle$, $|5_1, 2_5\rangle$, and $|6_1, 2_5\rangle$. The lack of curvature indicates that the coefficient $2(D_{J'} - D_{J''})$ is much smaller than $2(B' - B'')$, consistent with values obtained for $|3_1\rangle$ and $|4_1\rangle$ by Bovey.[26] Error limits were determined from the standard deviation of the slope and intercept.

No strong perturbations are apparent in the spectra shown in Figs. 1 and 2, but this is almost certainly due to the low resolution and congestion in our spectra. Small perturbations in the $|3_1\rangle$ and $|4_1\rangle$ states of CHD_3 were observed with higher resolution by Bovey.[26] The increased density of vibrational states at the energies of these spectra makes the presence of perturbations likely.

A rotational analysis of the $|7_1\rangle$ state and the feature near 544.7 nm was not attempted. The low signal to noise and congestion found in the spectrum of Fig. 3 made this impossible. An approximate value of B' for the

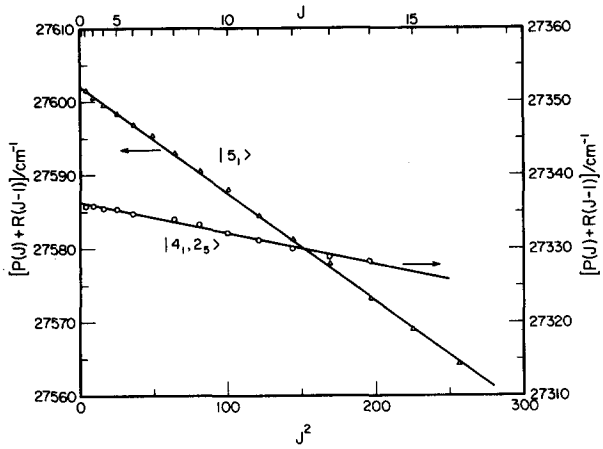

FIG. 5. Combination sum $P(J) + R(J-1)$ plot for CHD_3 vibrational states present in the spectrum of Fig. 1. Combination sums for $|5_1\rangle$ are indicated by the open triangle symbols and correspond to the ordinate scale on the left. Combination sums for $|4_1, 2_5\rangle$ are indicated by the open circle symbols and correspond to the ordinate scale on the right. All ordinate values are in vacuum wave numbers. The lines represent least-square fits to the data.

$|6_1, 2_5\rangle$ state is listed in Table VI, but is subject to large uncertainty. The extreme congestion between the $|7_1\rangle$ and $|6_1, 2_5\rangle$ states and the low signal-to-noise ratio makes the assignment of the individual J transitions in $|6_1, 2_5\rangle$ difficult. The slope of the combination sum line shown in Fig. 7 definitely is positive, however, indicating that B' for $|6_1, 2_5\rangle$ is larger than B''.

4. Discussion of rotational constants

Three attempts to explain the CHD_3 rotational constants obtained in this work are presented in the following three subsections. Only the third is able to qualitatively explain the observed data.

In trying to explain the CHD_3 rotational constants, we considered in succession interpretations based on: (a)

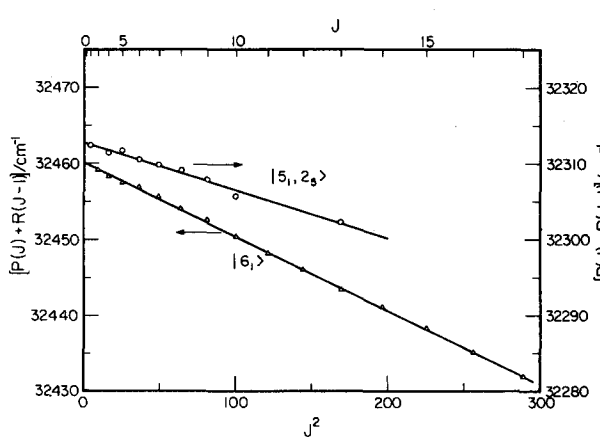

FIG. 6. Combination sum $P(J) + R(J-1)$ plot for CHD_3 vibrational states present in the spectrum of Fig. 2. Combination sums for $|6_1\rangle$ are indicated by the open triangle symbols and correspond to the ordinate scale on the left. Combination sums for $|5_1, 2_5\rangle$ are indicated by the open circle symbols and correspond to the ordinate scale on the right. All ordinate values are in vacuum wave numbers. The lines represent least-squares fits to the data.

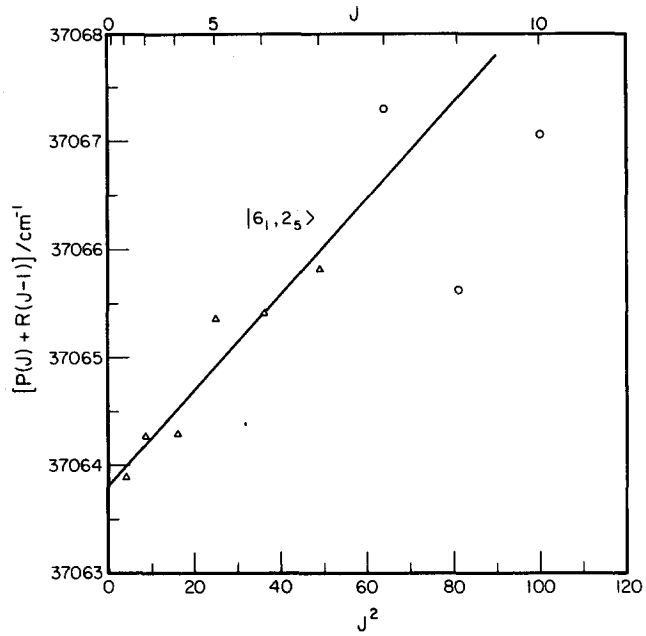

FIG. 7. Combination sum $P(J) + R(J-1)$ plot for CHD_3 state $|6_1, 2_5\rangle$. The points shown by open triangles were used in the least-squares fitting of the line for the combination sum analysis. The points shown by open circles correspond to strongly perturbed features in the spectrum of Fig. 3 and were not used in the combination sum analysis. The ordinate scale is in vacuum wave numbers.

noninteracting vibrational states, (b) two Fermi-interacting vibrational states, and (c) other interacting vibrational states. Although only the last was able to explain the data, information derived from the preceding two approaches was used in it. We will therefore describe all three.

a. Noninteracting states model. Figure 8 shows the known rotational constants from this work and previous work for vibrational states of CHD_3 of the form $|v_1\rangle$ and $|v_1, 2_5\rangle$. The rotational constant B' corresponds to the moment of inertia along an axis perpendicular to the C_{3v} symmetry axis. For transitions to states $|v_1\rangle$ with v_1 between 0 and 4, B'_v is essentially a linear function of v_1 in agreement with the standard expression[29(g)]

$$B_{[v_i]} = B_e - \sum_i \alpha_i^B \left(v_i + \frac{d_i}{2}\right). \tag{15}$$

$B_{[v_i]}$ is the rotational constant for the state designated by the set of vibrational quantum numbers $[v_i]$, B_e is the equilibrium rotational constant, the sum is over all vibrational modes, d_i is the degeneracy of the ith vibrational mode, and the α_i^B are small constants. The experimental value of α_1^B is 0.0160 cm^{-1}.[26] Noninteracting states of the form $|v_1\rangle$ should fall on this line.

B_{5_1} exhibits a slight positive deviation from this line and B_{6_1} is shifted substantially above the $\alpha_1^B = 0.0160$ cm^{-1} line. One explanation for this behavior is the presence of additional terms which are neglected in Eq. (15) of the form

$$-\sum_{i \geq j} \beta_{ij}^B \left(v_i + \frac{d_i}{2}\right)\left(v_j + \frac{d_j}{2}\right). \tag{16}$$

As the molecule approaches dissociation, however, vibrational coordinates lengthen rapidly and the $B_{[v_1]}$ curve should bend downward implying that β_{ii}^B should be positive. The points for B_{5_1} and B_{6_1} are above the straight line, implying that $\beta_{ii}^B < 0$. In addition, the size of the deviation for B_{6_1} cannot be accounted for by small higher order corrections. We conclude that the noninteracting states model does not explain the observed rotational constants.

b. Two Fermi-interacting states. A more plausible explanation for the rotational constants is the Fermi resonance between different zero order vibrational states. Figures 1 and 2 each show two states of the form $|v_1\rangle$ and $|(v-1)_1, 2_5\rangle$. As these states get closer together (Fig. 2) their intensities become comparable, a direct result of Fermi resonance between the two states (discussed above). For two interacting vibrational levels with zero-order rotational constants B_n^0 and B_i^0 which interact with Fermi mixing coefficients a and b the new rotational constants are given by[29(g)]

$$B_n = a^2 B_n^0 + b^2 B_i^0,$$
$$B_i = b^2 B_n^0 + a^2 B_i^0, \tag{17}$$

where $a^2 + b^2 = 1$.

The two new constants B_n and B_i are therefore intermediate between the zero order constants B_n^0 and B_i^0. The size of the shift from the zero order rotational constants to the new rotational constants reflects the amount of interaction between the vibrational levels. In the limit of equal mixing the constant should be the same for the two states.

In CHD_3 the CH bond is perpendicular to the axis corresponding to the B' constant. This explains why the excitation of the CH-stretch mode is so effective in increasing the moment of inertia I_B and therefore in decreasing B'. On the other hand, an increase in the CH bending mode (ν_5) vibration quantum number decreases the average distance between the H atom and the B axis, causing B' to increase. These qualitative considerations suggest that mixing in CH bend character from combination bands of the form $|(v-1)_1, 2_5\rangle$ with pure CH-stretch overtones of the form $|v_1\rangle$ effectively increases B'_{v_1} from its zero order α_i^B line, in agreement with our observation. The decrease in rotational constant between the $|4_1, 2_5\rangle$ and $|5_1, 2_5\rangle$ states also agrees qualitatively with the two-level Fermi mixing model, where the $|5_1, 2_5\rangle$ state interacts strongly with the $|6_1\rangle$ state.

This simple two-level Fermi mixing model, however, does not quantitatively account for the rotational constants of the combination band states of the form $|v_1, 2_5\rangle$. Allen and Plyler[22] have partially resolved the rotational structure of the A_1 component of the state $|2_5\rangle$. They report a value for B'–B'' of about 0.01 cm^{-1}. Using the Jennings and Blass[18] value for B'' we obtain $B'_{2_5} = 3.289$ cm^{-1} for that state. This value agrees closely with the result $B'_{2_5} = 3.288\,31$ cm^{-1} predicted from the Dupre-Maquaire *et al.*[21] measurement of $\alpha_5^B = -4.627 \times 10^{-3}$ cm^{-1} and

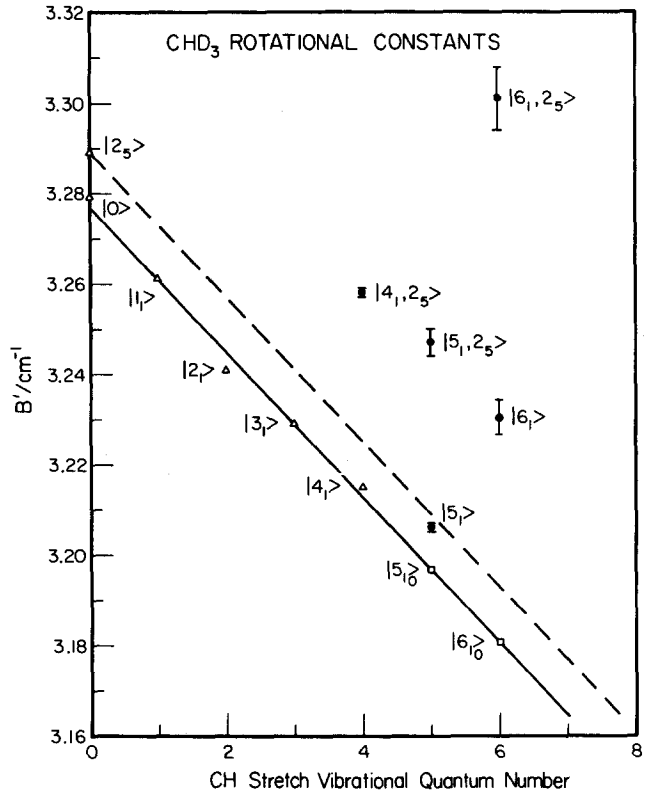

FIG. 8. CHD_3 rotational constants B' vs CH-stretch quantum number. The open triangle symbols correspond to previous studies (see Table II). The full circle symbols correspond to our data. The error bars represent ±2 standard deviations obtained from the least-squares fits of the combination sum analysis. The open square symbols correspond to zero order rotational constants. The solid line is the result of a least-square fit to the points for $|0\rangle$, $|1_1\rangle$, $|2_1\rangle$, $|3_1\rangle$, and $|4_1\rangle$ and represents the effects of the CH-stretch quantum number on the rotational constant B' for noninteracting vibrational states. The dashed line is a similar line obtained for states of the form $|v_1, 2_5\rangle$. The values for B' are in vacuum wave numbers.

Jennings and Blass's[18] value of $B'' = 3.279\,053$ cm^{-1}. The rotational constant $B_{v_1,2_5}$, in going from $B_{0_1,2_5}$ to $B_{4_1,2_5}$ or $B_{5_1,2_5}$ should only change by the α_1^B term in Eq. (15). The dashed line in Fig. 8 indicates this behavior which parallels the α_1^B line of the states $|v_1\rangle$.

The rotational constants $B_{4_1,2_5}$, $B_{5_1,2_5}$, and $B_{6_1,2_5}$ fall above this dashed line. If B_{2_5} is correct and only a two-level Fermi interaction occurred, all values for B_{v_1} and $B_{v_1,2_5}$ should have fallen either on or between the dashed line and the solid line, at least until higher order corrections like Eq. (16) become important.

c. Other interacting states. To obtain states with rotational constants above the dashed line of Fig. 8 it is necessary to mix in states with high rotational constant character. These additional states, which we have not observed, must consist of states from the bath of background states.

The information in Table II is useful in indicating which types of states are likely candidates for introducing higher rotational constant character into the observed spectra. In CHD_3, as energy is added into either the ν_1, ν_2, or ν_4 mode, the corresponding B rotational constants

decrease. In contrast, the one for ν_5 increases with increasing excitation energy ($\alpha_5^B > 0$). The behavior for ν_3 and ν_6 is not known. As a result, vibrational states in the region of our spectra which contain substantial amounts of ν_5 character are likely candidates for coupling which result in an increase of B.

The rotational constant for the state $|6_1, 2_5\rangle$ has large error limits but seems to also fall substantially above the dashed line in Fig. 8. This again implies a need for coupling to states of higher rotational constants, such as several weak coupling states or possibly the state appearing at 544.7 nm. Another possible mechanism (in addition to Fermi resonance) for coupling the observed states to states of high rotational B' constant is Coriolis coupling. Coriolis coupling of the allowed A_1 states and states of E symmetry (such as the E component of $|v_1, 2_5\rangle$) would lead to further mixing of the B' constant. We are unable to distinguish between these possibilities at the present.

5. Comparison with other CH-containing saturated molecules

Combination bands of the form $|v_{CH}, 2_{bend}\rangle$ have been observed in the high-energy CH-stretching overtone spectra of $CHCl_3$ and $CHBr_3$,[32] some lower alkanes,[34] haloethanes,[33] and dihalomethanes.[6] As shown by Fang and Swofford[32] the intensity of the combination band may be very large as a result of the Fermi resonance with a nearby pure CH-stretching overtone. They have analyzed the first-order shift of the combination band and obtained large negative anharmonic interaction constants: x_c (CH-str, bend) = -31 ± 3 cm^{-1} ($CHCl_3$); -24 ± 5 ($CHBr_3$). Interestingly, the same interaction constant obtained in this work for CHD_3 ($x_{15} = -19.5 \pm 3$ cm^{-1}) is somewhat smaller but comparable to the trihalomethane anharmonic constants. Similar values have been obtained for other molecules in the studies mentioned above.

Mortensen *et al.*[6] have performed a theoretical analysis of the anharmonic coupling of the CH-stretch and bending motions in the dihalomethanes based on an effective G matrix for the bending motion which accounts for the change in the effective mass for the bending motion when the CH stretch is excited. However, this analysis predicted a decrease in bending frequency with the number of CH-stretch quanta which was larger than that observed. This indicates, as they point out, that potential energy coupling is probably important also. From our analysis of the Fermi resonance in CHD_3 we also find fairly large interaction matrix elements for the CH-stretch–bend interaction. It will be interesting to determine the relative importance of kinetic and potential energy coupling terms in the theoretical description of the CHD_3 CH-stretch–bend interaction in the high-energy region.

B. Other deuterated methanes

We have also obtained the $\Delta v = 6$ CH-stretching overtone spectra (see Fig. 9) for other gaseous deuteromethanes: CH_2D_2, CH_3D, and CH_4. The spectrum of CH_4 [Fig. 9(c)] in this region has been obtained previously.[14,15] Our spectrum is in excellent agreement with the previous low resolution work, providing an independent check of our methodology.

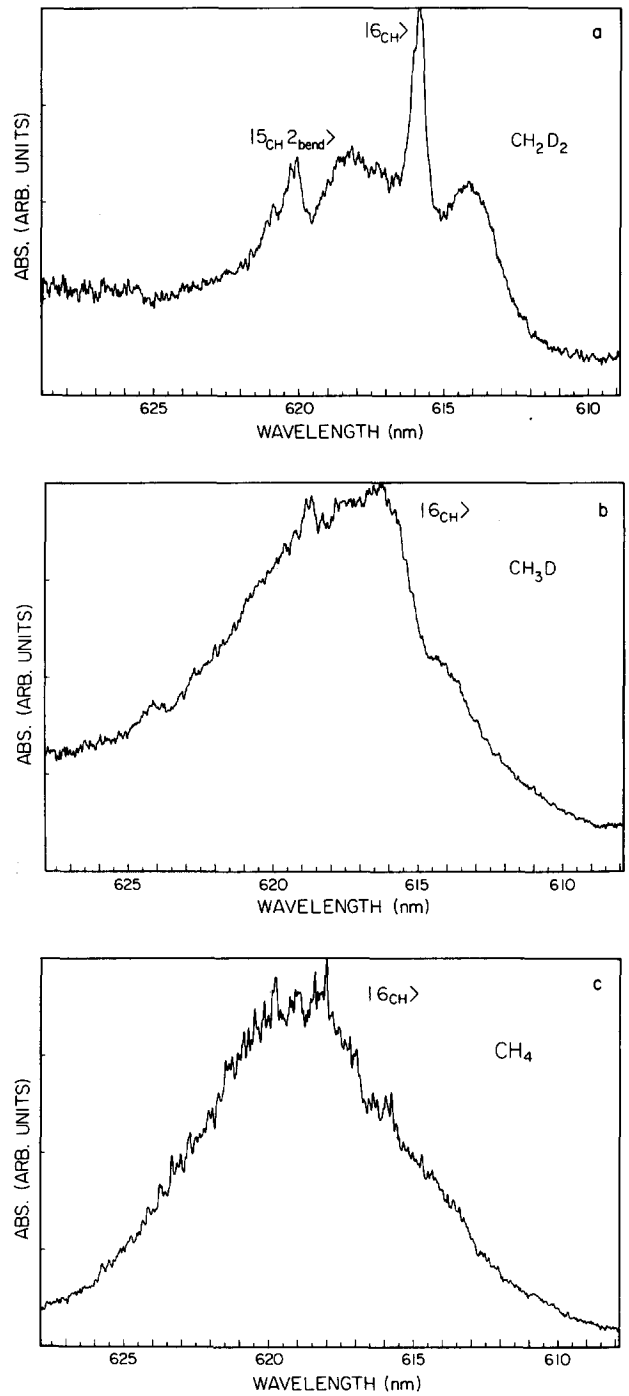

FIG. 9. Pulsed photoacoustic CH-stretching overtone spectra of (a) CH_2D, (b) CH_3D, and (c) CH_4 vapors in the $\Delta v_{CH} = 6$ region. All sample temperatures were ~25°. (a) The sample pressure was 330 Torr. The spectrum is an average of four scans. (b) The sample pressure was 370 Torr. The spectrum is an average of five scans. (c) The sample pressure was 300 Torr. The spectrum is an average of five scans.

The CH_2D_2 molecule is a very interesting one because of the different possible types of coupling. There exists a possibility for purely CH-stretching resonance and near-

resonance interactions between the identical CH modes, in addition to interactions between the CH stretch and other lower frequency modes as in the case of CHD_3. It is possible that CH_2D_2 can serve as a model system for assessing the degree of coupling of the two CH stretches in the high-energy region.

The spectrum presented in Fig. 9(a) is quite simple; there exist basically two vibrational bands at 16 238(5) and 16 124(5) cm^{-1}. The main band is broadened relative to CHD_3 and the rotational structure is washed out into simple P, Q, and R branch envelopes. This congestion is expected since the molecule is an asymmetric top with near degeneracy in the moment of inertia; the rotational structure at room temperature is complex, resulting in severe congestion of the lines which are not resolvable at our resolution. The other vibrational band is weaker and without well-defined rotational structure. As for the assignment, there are two general possibilities: either the states are, in local mode language, the symmetric and antisymmetric combinations (both of which are symmetry allowed from the ground state) of the $|6, 0\rangle$ states, where the two occupation numbers refer to the two local CH stretches, or one state is a pure local mode overtone, that is a superposition of the $|6, 0\rangle_\pm$ states, and the other state is some local-normal combination band. Without a complete study of the lower vibrational overtones it is not possible to give a definitive conclusion on this assignment. Some information is available from other studies which makes one possibility much more reasonable. First of all, the theory of the overtone spectroscopy for two identical coupled X–H oscillators which share a common X atom has been addressed for other molecules, for example for H_2O[4,5,36–38] and the dihalomethanes.[6] In the theoretical treatments, the local mode picture has been successfully used to describe the vibrational states of the two stretching oscillator system ranging from low ($\Delta v = 1,2$) to higher energy ($\Delta v \geq 3$). This picture uses, as a basis, the properly symmetrized combinations of local bond stretching functions. The splitting of these symmetric and antisymmetric stretching states results primarily from direct coupling of the oscillators for $\Delta v = 1$ and through mixing with higher energy vibrational configurations (symmetrized local–local combinations) for $\Delta v \geq 2$. Since for higher energy states there is very weak direct first order coupling and since the splitting of symmetrized local–local combinations from the symmetrized overtone increase with increasing v (due to the large bond anharmonicity), it is found that the net splitting of the local mode doublets decreases with increasing v under particular conditions (magnitude of interbond coupling < bond anharmonicity) thus resulting in increased localization of the vibrational energy with increasing v.

The splitting of the fundamentals, $|1, 0\rangle_\pm$ gives twice the interaction energy (x_{12}) of the CH oscillators, as is found by diagonalizing the appropriate 2×2 energy matrix. The CH-stretching fundamentals of CH_2D_2 have been studied previously.[39] The energy of the $|1, 0\rangle_\pm$ states were found to be 2975.5 cm^{-1} ($|1, 0\rangle_+$) and 3012 cm^{-1} ($|1, 0\rangle_-$). The splitting is 36.5 cm^{-1} and therefore the interbond coupling energy is $x_{12} = 18.2$ cm^{-1}. To estimate the bond anharmonicity we use the average energy of the $|1, 0\rangle_\pm$ states (2993.7 cm^{-1}) and the observed energy of the higher intensity transition in the $\Delta v_{CH} = 6$ region (16 238 cm^{-1}) along with the simple Birge–Sponer relationship: $\Delta E = \bar{\nu} v + x v^2$. We find that $\bar{\nu} \sim 3052$ cm^{-1} and that x, the bond anharmonicity is ~ -58 cm^{-1}. Thus for CH_2D_2 we see that $|x_{12}| < |x|$ and we would expect the splitting of $|v, 0\rangle_\pm$ states to decrease with increasing v. The states observed in the $v = 6$ region are split by 144 cm^{-1}, which is much larger than the 36.5 cm^{-1} fundamental splitting. On this basis it is much more reasonable to assign the higher energy band as due to unresolved absorption to $|6, 0\rangle_\pm$ and the weaker lower energy band to a combination band of the form $|5, \{v_i\}\rangle$, where $\{v_i\}$ refers to a set of quanta in non-CH-stretching modes. We can now put an upper limit on the splitting of the $|6, 0\rangle_+$ and $|6, 0\rangle_-$ states of <10 cm^{-1}. Since symmetric (A_1) and antisymmetric (B_1) overtone states are allowed in electric dipole absorption for CH_2D_2, then combination states of A_1 or B_1 symmetry can mix via Fermi resonance with the corresponding overtone of the same symmetry. Several possible combination states exist which have correct symmetry, approximately correct energy and can mix with $|6_{CH}\rangle$ via low order terms; these include $|5_{CH}, 2_9\rangle$ and $|5_{CH}, 1_3 + 1_4\rangle$. Accurate calculations of the energies are required to make a definite assignment.

The spectra of gaseous CH_3D and CH_4 shown in Figs. 9(b) and 9(c) are apparently much more congested than the spectra of CH_2D_2 and CHD_3 at the same quantum level. For CH_3D, a feature at longer wavelength than the main band peak can be seen. It is possible that this feature is a combination band similar to the longer wavelength band in the CH_2D_2 spectrum, but suffers greater overlap with the main band. The small band at shorter wavelength is probably the envelope of the R branch of the main vibrational band.

The CH_3D overtone spectrum will be comprised primarily of A_1 and E symmetry-adapted combinations of the local mode basis states $|v, 0, 0\rangle$, $|0, v, 0\rangle$, and $|0, 0, v\rangle$ where the occupation numbers refer to the three CH stretches.[40] However, since the $CH_3D\Delta v_{CH} = 6$ spectrum is even more congested than the CH_2D_2 spectrum, it is not possible to put a meaningful upper limit on their splitting. Therefore for simplicity we resort to the local mode labels for assignment. The main band is identified as $|6_{CH}\rangle$ and some possibly nearby combination states are $|5_{CH}, 2_3\rangle$, $|5_{CH}, 1_3, 1_6\rangle$, $|5_{CH}, 1_5, 1_6\rangle$, and $|5, 2_6\rangle$ again using the mode numbering of Ref. 31.

The CH_4 overtone spectrum is described[41] in terms of A_1 and T_2 symmetry adapted combinations of the local mode states of which the T_2 state is electric dipole allowed. However, the $CH_4\Delta v = 6$ spectrum [Fig. 9(c)] is the most congested spectrum obtained in this study of some isotopic methanes. The low resolution spectrum obtained here does not allow identification of the number of band systems that are present. At higher resolution it is found that the band is made up of resolvable features,[14,15] but no identification of the various bands was given.

From our studies of various deuteromethanes at $\Delta v_{CH} = 6$, we conclude that the spectrum is not only rotationally congested but is probably vibrationally congested as well, probably involving two and possibly more band systems, the pure stretching overtone $|6_{CH}\rangle$ and combinations built on $|5_{CH}\rangle$, for example $|5_{CH}, 2_4\rangle$. However, the complete mechanism which results in the observed congested spectrum is still an unresolved issue.

IV. CONCLUSIONS

We now summarize the conclusions reached in this work.

(1) The high-energy overtone spectra ($\Delta v_{CH} = 5$, 6, and 7) of CHD_3 are strongly affected by Fermi resonance of the pure overtone $|v_{CH}\rangle$ with combinations $|v_{CH} - 1, 2_5\rangle$ (and $|v_{CH} - 1, 1_5, 1_6\rangle$ for $\Delta v_{CH} = 7$). The spectra are reasonably well described using degenerate perturbation theory. This analysis yields values for some of the interaction matrix elements and first-order energies of the combination bands. There are large first-order shifts of the combination bands which also result from interactions of the CH-stretch and bending vibrations. The shift is roughly in agreement with the scaling with v_{CH} given by first-order perturbation theory. Relatively congested spectra are obtained for the $v_{CH} = 7$ region which indicate that in this region there is extensive vibrational mixing.

(2) The fair success of the simple analysis of the CHD_3 overtone spectra in terms of Fermi resonances is in contrast with the failure of such an approach to describe the derived excited state rotational constants. This discrepancy is rationalized in terms of interactions with other weakly coupled combinations of high rotational B' constant via Fermi resonance or Coriolis coupling.

(3) The laser limited linewidths obtained for CHD_3 show that this small molecule does not undergo rapid intramolecular vibrational redistribution as is believed to occur in larger molecules[43] such as benzene.

(4) The spectrum of CH_2D_2 in the region around $v_{CH} = 6$ indicates two bands which are assigned in analogy with the bands of CHD_3. There is no splitting observed in the $|6_{CH}\rangle_{\pm}$ states. This observation allows an upper limit (determined by the width of the Q branch) of the splitting of ~ 10 cm^{-1} to be established. This result is in agreement with the results of other work (*vide supra*) which indicate similar small splittings of the symmetrized local mode states for several two CH oscillator molecules.

(5) Comparison of the $v_{CH} = 6$ spectra of CHD_3, CH_2D_2, CH_3D, and CH_4 indicate increasing spectral congestion with increasing numbers of hydrogens. Rotational and vibrational congestion have been implicated; however, further work is required to identify the actual mechanism of congestion.[42]

Very recently, the high resolution spectra of CHD_3 at $v = 6$ have been obtained by Scherer, Lehmann, and Klemperer at Harvard.[44] The spectra at 77 K show fully resolved K structure and Doppler limited linewidths. The derived rotational B' constants are in good agreement (though of higher accuracy) with the ones derived in our work. As a final note we would like to point out that the lower energy states (800–10 000 cm^{-1}) of CHD_3 have been studied recently by Quack and co-workers.[45] In private communication we learned that by using their results they predicted higher energy states that are in reasonable agreement with our results. Theoretical calculations employing both kinetic and potential coupling terms of the Hamiltonian for the high-energy overtone and combination states of CHD_3 and CH_3D will be described in a forthcoming paper.[46]

ACKNOWLEDGMENTS

AHZ would like to thank Professor R. Zare and Dr. D. Chandler for communicating unpublished results on gas phase halomethanes during a visit to Stanford University. We gratefully thank Professor K. Janda and Professor R. Marcus for discussions, Dr. J. J. Barret for the help with the design of the photoacoustic cell and Professor J. Beauchamp for providing us with some samples used in these studies. We would also like to thank Dr. K. Lehmann and Dr. A. Pine for comments and suggestions. This work was supported in part by grants from the National Science Foundation (Grant No. CHE-8211356) and the U.S. Department of Energy (Contract No. DE-AS03-765F00767).

[1] B. R. Henry, Acc. Chem. Res. **10**, 207 (1977).
[2] For reviews see (a) B. R. Henry, Vib. Spectra Struct. **10**, 269 (1981); (b) M. L. Sage and J. Jortner, Adv. Chem. Phys. **47**, 293 (1981); (c) H. L. Fang and R. L. Swofford, *Advances in Laser Spectroscopy*, edited by B. A. Garetz and J. R. Lombardi (Heyden, London, 1982), Vol. 1.
[3] M. S. Burberry and A. C. Albrecht, J. Chem. Phys. **71**, 4631 (1979).
[4] H. S. Moller and O. Sonnich Mortensen, Chem. Phys. Lett. **66**, 539 (1979).
[5] R. T. Lawton and M. S. Child, Mol. Phys. **40**, 773 (1980).
[6] O. Sonnich Mortensen, B. R. Henry, and M. Ali Mohammadi, J. Chem. Phys. **75**, 4800 (1981).
[7] J. W. Perry and A. H. Zewail, J. Phys. Chem. **85**, 933 (1981); **86**, 5197 (1982).
[8] K. V. Reddy, D. F. Heller, and M. J. Berry, J. Chem. Phys. **76**, 2814 (1982).
[9] J. W. Perry and A. H. Zewail, J. Chem. Phys. **70**, 582 (1979); Chem. Phys. Lett. **65**, 31 (1979).
[10] D. J. Moll and A. Kuppermann (to be published).
[11] G. A. West, D. R. Siebert, and J. J. Barrett, J. Appl. Phys. **51**, 2823 (1980).
[12] S. L. Chin, D. K. Evans, R. D. McAlpine, and W. N. Selander, Appl. Opt. **2**, 65 (1982).
[13] L. P. Giver, J. Quant. Spectrosc. Radiat. Transfer **19**, 311 (1978).
[14] G. Stella, J. Gelfand, and W. H. Smith, Chem. Phys. Lett. **39**, 146 (1976).
[15] J. Gelfand, W. Hermina, and W. H. Smith, Chem. Phys. Lett. **65**, 201 (1979).
[16] L. Darton and J. S. Margolis, J. Quant. Spectrosc. Radiat. Transfer **13**, 969 (1973).
[17] J. S. Margolis, J. Quant. Spectrosc. Radiat. Transfer **11**, 69 (1971).
[18] D. E. Jennings and W. E. Blass, J. Mol. Spectrosc. **55**, 445 (1975).
[19] H. W. Kattenberg and S. Brodersen, J. Mol. Spectrosc. **59**, 126 (1976).
[20] J. K. Wilmhurst and H. J. Bernstein, Can. J. Chem. **35**, 226 (1957).
[21] J. Dupre-Maquaire, J. Dupre, and G. Tarrago, J. Mol. Spectrosc. **90**, 63 (1981).

[22] H. C. Allen, Jr. and E. K. Plyler, J. Res. Natl. Bur. Stand. Sect. A **63**, 145 (1959).
[23] D. G. Rea and H. W. Thompson, Trans. Faraday Soc. **52**, 1304 (1956).
[24] W. F. Blass and T. H. Edwards, J. Mol. Spectrosc. **24**, 16 (1967).
[25] T. A. Wiggins, E. R. Shull, J. M. Bennett, and D. H. Rank, J. Chem. Phys. **21**, 1940 (1953).
[26] L. F. H. Bovey, J. Chem. Phys. **21**, 830 (1953).
[27] The CHD_3 molecule is a special case in that the CH-stretch internal coordinate is directed along the principal symmetry axis of the molecule, therefore the CH-stretch coordinate is totally symmetric for either a local or normal mode model. The state symmetries and selection rules for C_3v will hold for either model.
[28] W. S. Benedict, K. Morikawa, R. S. Barnes, and H. S. Taylor, J. Chem. Phys. **5**, 1 (1937).
[29] G. Herzberg, *Infrared and Raman Spectra* (Van Nostrand, Princeton, 1945), (a) p. 215, (b) p. 210, (c) p. 400, (d) p. 26, (e) p. 421, (f) p. 391, (g) p. 378.
[30] E. B. Wilson, J. Decius, and P. Cross, *Molecular Vibrations* (McGraw-Hill, New York, 1955), p. 197.
[31] D. L. Gray and A. G. Robiette, Mol. Phys. **37**, 1901 (1979).
[32] H. L. Fang and R. L. Swofford, J. Chem. Phys. **72**, 6382 (1980).
[33] B. R. Henry and M. Ali Mohammadi, Chem. Phys. **55**, 385 (1981).
[34] H. L. Fang and R. L. Swofford, J. Chem. Phys. **73**, 2607 (1980).
[35] J. L. Duncan, D. Ellis, and I. J. Wright, Mol. Phys. **20**, 673 (1971).
[36] R. Wallace, Chem. Phys. **11**, 189 (1975).
[37] M. L. Elert, P. R. Stannard, and W. M. Gelbart, J. Chem. Phys. **67**, 5395 (1977).
[38] A. A. Ovchinnikov and N. S. Erikman, Opt. Spectrosc. **34**, 690, 887 (1973).
[39] J. C. Deroche and G. Guelachvilli, J. Mol. Spectrosc. **56**, 76 (1975).
[40] L. Halonen and M. S. Child, J. Chem. Phys. **79**, 4355 (1983).
[41] L. Halonen and M. S. Child, Mol. Phys. **46**, 239 (1982).
[42] We have also studied neopentane and tetramethylsilane in the gas phase and observed no rotational structure; instead the bands observed are very broad. For more details see Ref. 44.
[43] J. W. Perry, Ph.D. thesis, California Institute of Technology, 1984.
[44] G. J. Scherer, K. K. Lehmann, and W. Klemperer (preprint).
[45] H. R. Dübal, M. Lewerenz, and M. Quack, Faraday Discuss. Chem. Soc. **75**, 358 (1983).
[46] G. A. Voth, R. A. Marcus, and A. H. Zewail, J. Chem. Phys. **81**, 5494 (1984).